Aberration correction in 2D echocardiography

Svein-Erik Måsøy, Bastien Dénarié, Anders Sørnes, Espen Holte, Bjørnar Grenne, Torvald Espeland, Erik Andreas Rye Berg, Ole Marius Hoel Rindal, Wayne Rigby, and Tore Bjåstad

***Abstract*— An aberration correction algorithm has been implemented and demonstrated in an echocardiographic clinical trial using 2D imaging. The method estimates and compensates arrival time errors between different sub-aperture processor signals in a matrix array probe in post processing. Five standard views of channel data cineloops were recorded from 22 patients. Using a coherence metric, the aberration correction algorithm was shown to improve image quality in all 7380 processed frames. In a blinded and left-right-randomized side-by-side evaluation, four cardiologists (two experienced and two in training) preferred the aberration corrected image in 97 % of the cases. The feedback from the clinicians was that the images appeared sharper with better contrast and less noise. Many structures like valve leaflets, chordae, endocardium, and endocardial borders appeared narrower and more clearly defined in the aberration corrected images. An important finding is that aberration correction improves contrast between the endocardium and ventricle cavities for all processed images. This was confirmed by the cardiologists in their feedback, and quantified with a median global gain difference estimate between the aberration-corrected and non-corrected images of 1.2 dB.**

***Index Terms*— ultrasound, aberration correction, speed of sound variations, beamforming, echocardiography**

I. Introduction

In medical ultrasound image reconstruction, the speed of sound in tissue is a vital parameter for image quality. The industry standard for tissue speed of sound in pulse-echo ultrasound systems is 1540 m/s. This represents an average value over different tissue types [1] and is set to a constant for all patients in most systems. Some commercial systems allow the user to manually choose a sound speed or can automatically change it for improved image reconstruction.

State-of-the-art ultrasound probes contain arrays of hundreds (2D imaging probes) or thousands of elements (3D imaging probes). The first step in array-based image reconstruction is focusing, aligning the received ultrasound wave emanating from a point in the body across the array elements. Due to propagation path differences, the wave arrives at each element at different times. By removing these arrival time differences, the wave can be coherently summed over all elements to provide a strong signal from a given point. If the speed of sound in the medium is constant and known, this focusing results in high resolution and contrast when the process is repeated for all spatially sampled points in an image. Assuming an erroneous constant speed of sound, degrades image quality [2], [3].

However, it is well known that different tissue types have different sound speeds [1], [4], [5]. This leads to arrival-time errors over the array elements when a constant speed of sound is assumed during focusing. The arrival-time errors, or *aberrations*, degrade image quality (both resolution and contrast) due to a lowered coherence in the element summation process. Aberrations also affect the transmitted ultrasound wave, yielding a less focused ultrasound beam with a wider main-lobe and increased sidelobe level [6]. The process of correcting for arrival time errors (and potentially amplitude variations) caused by heterogeneous tissue on receive, or both transmit and receive, is referred to as *aberration correction*.

Large local variations of the speed of sound are typically found in the body wall, which consists of the skin, subcutaneous fat, connective tissue, and interleaved muscle and fat layers with velocities varying from 1478 m/s in fat, 1547 m/s in muscle, to 1613 m/s in connective tissue [7]. A series of studies have been performed to characterize aberrations generated by the body wall. These studies used excised human tissue for quantification of aberrations both *in vivo* and *in silico* from the abdominal wall [7]–[10], the breast [11], and chest wall [12]. The degree of aberration varies between the different body wall types and is correlated with its thickness [12]. In the chest wall, aberrations are effectively increased by interaction of the ultrasound field with the ribs, which is dependent on the intercostal spacing [12].

Obesity, which increases the thickness of the body wall, leads to a significant reduction in images rated as ”good” and an increase in those rated as ”poor” [13]. It also leads to more use of contrast enhanced ultrasound (CEUS) and trans-esophageal echocardiography (TEE) in order to improve assessment of heart function [14].

Research into methods for compensating aberrations in pulse-echo imaging has been ongoing for more than 40 years. A selected number of papers on this topic is provided in Refs. [15]–[29]. Many of these methods have been tested in lab

“This work was supported by the Centre for Innovative Ultrasound Solutions under the Research Council of Norway Project Code 237887.”

Svein-Erik Måsøy, Espen Holte, Bjørnar Grenne, Torvald Espeland, Erik Andreas Rye Berg, and Tore Bjåstad are with The Department of Circulation and Medical Imaging, Norwegian University of Science and Technology (NTNU), Trondheim, Norway (Corresponding author e-mail: svein-erik.masoy@ntnu.no).

Espen Holte and Bjørnar Grenne, Torvald Espeland, Erik Andreas Rye Berg are also with the St. Olavs hospital, Trondheim University Hospital, Trondheim, Norway.

Bastien Dénarié and Anders Sørnes are with GE Vingmed Ultrasound AS, Horten, Norway.

Ole Marius Hoel Rindal is with the University of Oslo, Oslo, Norway.

Wayne Rigby is with GE Research, Niskayuna, NY, USA.

Tore Bjåstad is also with InPhase Solutions AS, Trondheim, Norway, and his contributions to this work has been as an employee of GE Vingmed Ultrasound AS and for the last years as a consultant for GE Healthcare from InPhase Solution AS and part time employee at NTNU.

settings or on a few selected clinical images but have not yet been implemented real-time in a clinical commercial system or validated in clinical trials with many patients.

In 2000, Rigby *et al.* [30] demonstrated real-time aberration correction in abdominal imaging in 13 healthy males using a multi-row abdominal probe. The results showed small but significant image improvements, such as improved visibility and contrast of known abdominal structures, reduced clutter in blood vessels, and improved brightness of liver tissue.

The motivation for this study is to evaluate image quality improvements with an aberration correction algorithm in a 2D transthoracic echocardiography (TTE) clinical trial with 22 patients from the St. Olavs hospital, Trondheim University Hospital (Trondheim, Norway). The aberration correction algorithm, named *Adapt*, is the result of a collaborative project between GE Healthcare and researchers at the Norwegian University of Science and Technology (Trondheim, Norway) and has been developed and implemented to run real-time in a GE Vivid E95 ultrasound system (GE Vingmed Ultrasound AS, Horten, Norway). The core of the Vivid E95 system is a software beamforming platform (*cSound*), meaning that all beamforming and image processing is implemented in software using CPUs and GPUs. The computing power of cSound allows for implementation of Adapt at imaging rates of more than 150 frames per second using factory settings for adult cardiac scanning sectors. For this study, ultrasound channel data were recorded and then post-processed with and without Adapt. This allowed for a side-by-side comparison of images processed from the same channel data cineloops. Image quality improvements were quantified with a coherence metric and by four clinicians.

II. Methods

A. Aberration correction algorithm

The aberration correction algorithm is implemented using the 4Vc-D matrix array probe (GE Vingmed Ultrasound AS, Horten, Norway) and can be used in both fundamental and harmonic imaging modes. This probe has a sub-aperture processor (SAP) structure, where element signals are pre-beamformed in the probe handle into 192 channels distributed over the array aperture. The Vivid E95 system can store ultrasound data from each SAP in the 4Vc-D probe prior to beamforming and further image processing. Such data are here referred to as channel data. In this study, the algorithm is applied off-line to the captured channel data.

The principle of the algorithm is to estimate arrival time errors between all SAP channels in the matrix array and to apply these as corrections in the image reconstruction process. As described in the introduction, the goal of aberration correction is to align the received signal across all SAP channels in the focusing step, reducing the effect of unknown sound speed variations from the body wall and increasing both image resolution and contrast.

B. Data collection and processing

Twenty-two patients (11 women and 11 men) were recruited over three working days in the Clinic of Cardiology at St. Olavs hospital during two weeks of October 2020. The patients had a minimum, median, and maximum age of 54, 72, 86 years respectively. The different recording days represented normal days in the clinic. Inclusion criteria were simply the willingness to participate in the study, age above 18 years, and a clinical indication for a TTE. Exclusion criteria were hemodynamically unstable patients, patients with arrhythmia, or lack of competent consent. The study was approved by the Regional Committee for Medical and Health Research Ethics of Mid-Norway (project number 142295), and all patients provided written consent.

For each patient, at least one cineloop containing at least one heart cycle was recorded for the five standard 2D views: parasternal long axis (PLAX), parasternal short axis (PSAX), apical four chamber (A4C), apical two chamber (A2C), and apical long axis (ALAX). Some patients had several recordings of the same cardiac view, and for some patients all five views were not recorded due to technical difficulties in the clinic. Default Vivid E95 factory settings for the 4Vc-D probe were used with the *Cardiac_E* application (harmonic imaging mode). All data were recorded by two senior cardiologists (B.G. and E.H.) with 7 and 11 years of experience as consultant cardiologists. In order to automatically classify cardiac views, a machine learning based view classifier developed by Østvik *et al.* [31] was used with a reported accuracy of 98.9 ± 0.6.

The recorded data were post-processed using a stand-alone workstation computer with a version of the Vivid E95 *cSound* beamforming and image processing software implemented in MATLAB (The Mathworks, Inc., Natick, MA, USA). This code is not CE or FDA approved. It encompasses all state-of-the-art image reconstruction and post-processing steps normally performed on the Vivid E95 system.

Each channel data cineloop was processed in two different ways:

1) Standard cSound processing, yielding conventional images as displayed by the E95 system during real-time scanning and here referred to as *standard images*.
2) Aberration correction inserted into the cSound processing, yielding aberration corrected images (also abbreviated *Adapt images*).

All other processing steps were identical for the images except for the global gain adjustment described in the next section. This allowed for side-by-side comparison of images processed with and without aberration correction from the same channel data cineloops. A total of 116 cineloops, consisting of 7380 individual frames, were recorded and processed to a DICOM format for display and clinical evaluation in *EchoPAC* (GE Vingmed Ultrasound AS, Horten, Norway), a stand-alone image evaluation and analysis software package provided with the Vivid E95 system.

C. Gain compensation

The aberration correction algorithm typically increases the signal intensity of the cardiac tissue. This leads to a systematic gain increase in the aberration corrected images, which was compensated for in order for the images to appear equalized with respect to global gain settings. The display gain for

the aberration corrected images was reduced to minimize the difference in intensity with the corresponding standard image.

The difference in intensity of the 20% brightest pixels between the aberration corrected and standard image was averaged over all 64 frames and used as a global gain reduction for the Adapt images. After this compensation, the images appeared to have similar global gain.

D. Image quality parameter

Image quality improvement was quantified in two ways.

First, an image quality metric based on signal coherence was developed. The received channel signal on SAP m in azimuth and n in elevation, with focusing delays applied to the data (with or without aberration correction delays), for an image pixel (x, z) may be defined as

$$s \equiv s_{mn}(x, z) \ . \tag{1}$$

The Coherence Factor (CF) [32], [33], the ratio between the coherent and incoherent sums over the channel signals, is

$$\mathrm{CF}(x, z) = \frac{\left| \sum_{m=1}^{M} \sum_{n=1}^{N} s_{mn}(x, z) \right|^2}{MN \sum_{m=1}^{M} \sum_{n=1}^{N} |s_{mn}(x, z)|^2} \ , \tag{2}$$

where x and z are the azimuthal and range coordinates of a beamformed pixel, and M and N are the number of azimuthal and elevational SAPs.

The Coherence Factor yields a normalized ultrasound image with values ranging from zero to one; it is a measure of how similar signals returning to each transducer element are. A value of one indicates equal signals returning at the same time (fully correlated). As arrival-time errors increase, however, the signals are no longer aligned and CF decreases. A similar decrease occurs for speckle-like reflectors, for which the signals are no longer identical. An image quality parameter termed the Global Image Coherence (GIC) was then defined as the CF averaged over all azimuthal pixels $1 < x < X$ and range pixels $Z_1 < z < Z$ in an image frame, where X and Z are the total number of azimuthal and range pixels, respectively:

$$\mathrm{GIC} = \frac{1}{X(Z - Z_1)} \sum_{x=1}^{X} \sum_{z=Z_1}^{Z} \mathrm{CF}(x, z). \tag{3}$$

In this work $Z_1 = Z/3$ to avoid potential near-field reverberations. The GIC can also be averaged over all frames in a cineloop, here referred to as the *average* GIC.

Second, an evaluation of image quality improvement was carried out by four clinicians, two senior cardiologists (B.G. and E.H.), and two fellows in cardiology (T.E. and E.A.R.B.), both with 10 years of experience with echocardiography. Images with and without aberration correction were displayed side-by-side in EchoPAC, randomized to the left or the right side for each recording. Since both the aberration corrected and non-corrected (standard) images were processed from the same channel data cineloop, they could be displayed with frame synchronization. This allowed for individual frame-to-frame comparison in addition to viewing the synchronized cineloops in replay mode.

The clinicians were instructed to select the preferred cineloop for all 116 pairs of processed patient recordings, or to judge them equal. The protocol stated the clinicians could reduce the replay speed of the paired cineloops, or freeze the cineloops and step through at most 10 consecutive synchronized paired frames. They could also adjust the display gain, which was applied equally to both cineloops. No specific image quality criteria were defined or agreed upon in advance. All the clinicians were made aware of the principles of aberration correction and that it may potentially improve the images.

III. Results

The relative increase in the GIC parameter after aberration correction from all frames and all subjects is shown in Fig. 1. The value is positive for all processed frames, indicating that all images obtain an improvement in image quality after aberration correction is applied.

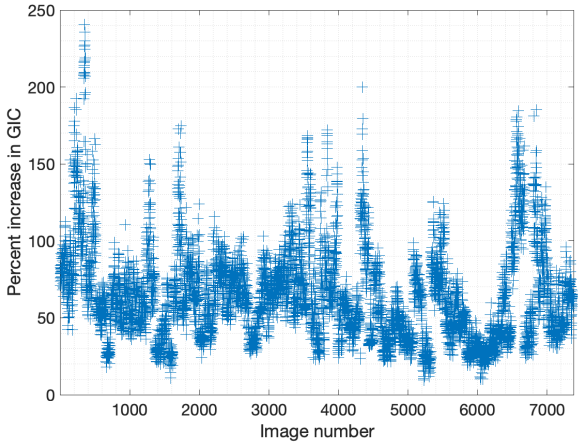

Fig. 1. Percentage increase in GIC after aberration correction for all 7380 processed frames.

Table I presents the results of the side-by-side preferred image analysis carried out by the clinicians. Of the 116 analyzed cineloops, the clinicians preferred the aberration corrected cineloops 97 % of the time. Two of the clinicians preferred the aberration corrected cineloops all the time (one experienced and one fellowed), whereas the two others preferred the standard processed cineloop in 11 instances. One cineloop was deemed to be of indistinguishable quality by one clinician.

Figure 2 shows average GIC (GIC averaged over all frames in one cineloop) for the standard images and the aberration corrected images, together with the average percentage increase in GIC after aberration correction and the gain compensation value applied to all cineloops. The horizontal axis displays the patient number and image view. The legend in this figure indicates the numbering of the image case examples presented in Figs. 4, 5, 6, and 7. The dotted line in each plot indicates the median value of each parameter.

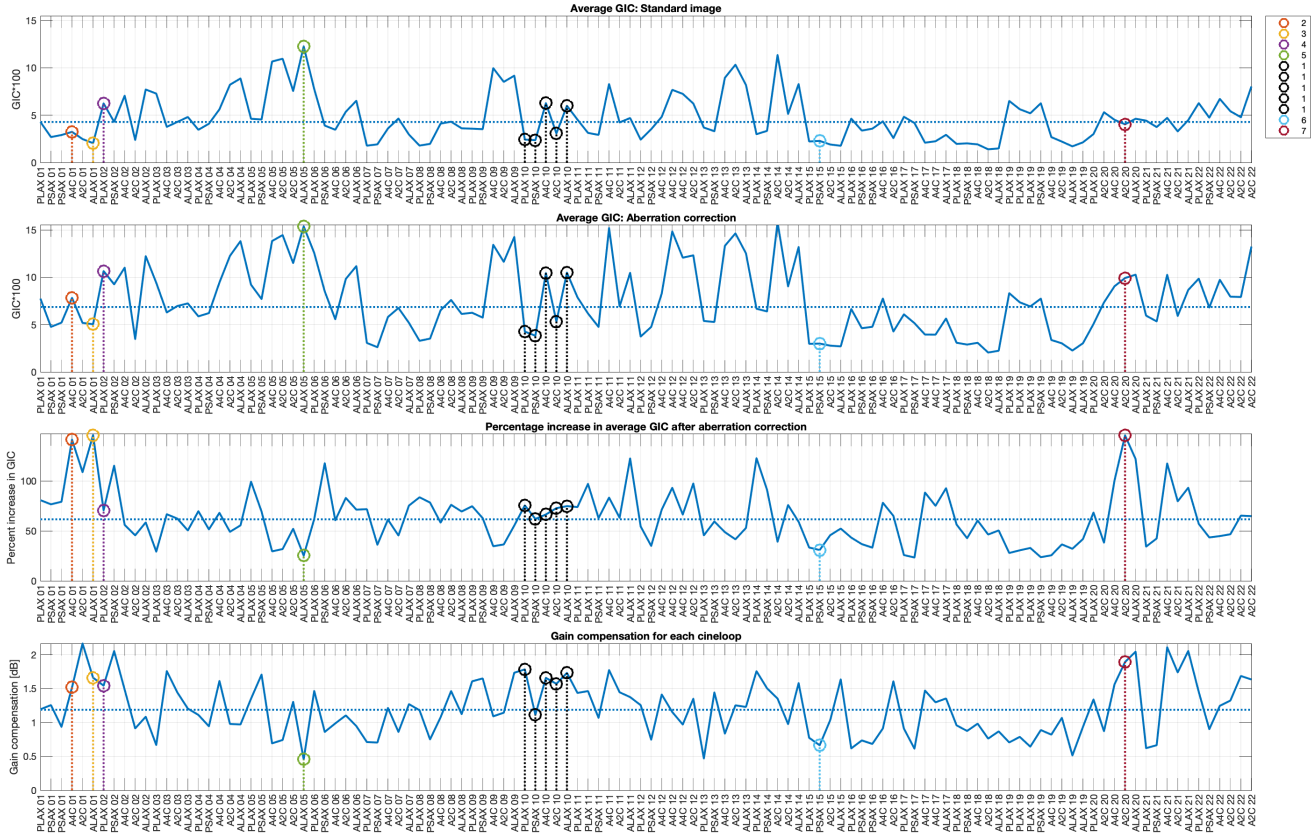

Fig. 2. Average GIC values and gain compensation over all frames in each recorded cineloop . Top row, average GIC before aberration correction. Second row, average GIC after aberration correction. Third row, the percentage increase in the average GIC parameter after aberration correction. Fourth row, estimated gain compensation value for each cineloop. The dotted line in each plot indicates the median value of each parameter. The x-axis display the patient number and corresponding detected image view. The legend shows the numbering of the image case examples presented in Figs. 4, 5, 6, and 7.

Clinician	Standard image	Adapt image	Equal
1	0	116	0
2	4	111	1
3	0	116	0
4	7	109	0
Sum	11	452	1
Percentage of all	2.4	97.4	0.2

TABLE I

PREFERRED IMAGE IN SIDE-BY-SIDE COMPARISON FOR ALL FOUR CLINICIANS. THE *Adapt image* COLUMN REFERS TO THE ABERRATION CORRECTED IMAGE. THE TWO LAST ROWS SUMMARIZE THE RESULTS AS THE ACCUMULATED SUM FOR EACH COLUMN, AND THE PERCENTAGE OF EACH CATEGORY WITH RESPECT TO ALL EVALUATED CINELOOPS.

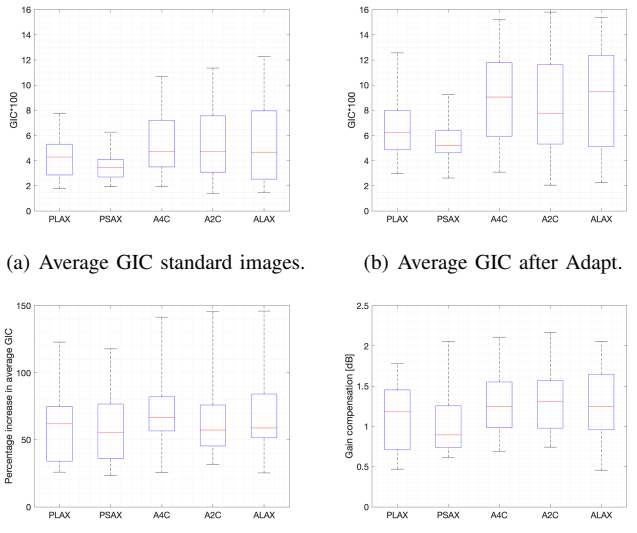

(a) Average GIC standard images. (b) Average GIC after Adapt.

(c) Increase in average GIC. (d) Gain compensation.

Fig. 3. Average GIC before and after aberration correction, percentage increase in average GIC after aberration correction, and gain compensation as a function of image view.

The median increase in GIC after aberration correction is 62 %, and the median value of the applied gain compensation is 1.2 dB. The Pearson linear correlation coefficient between the average GIC ratio increase and the gain compensation is 0.67, indicating a significant correlation between these parameters.

The parameters from Fig. 2 are sorted by view in Fig. 3. There was no statistical difference in GIC increase by view.

In Figs. 4 and 5, a selected frame from all 5 recordings of

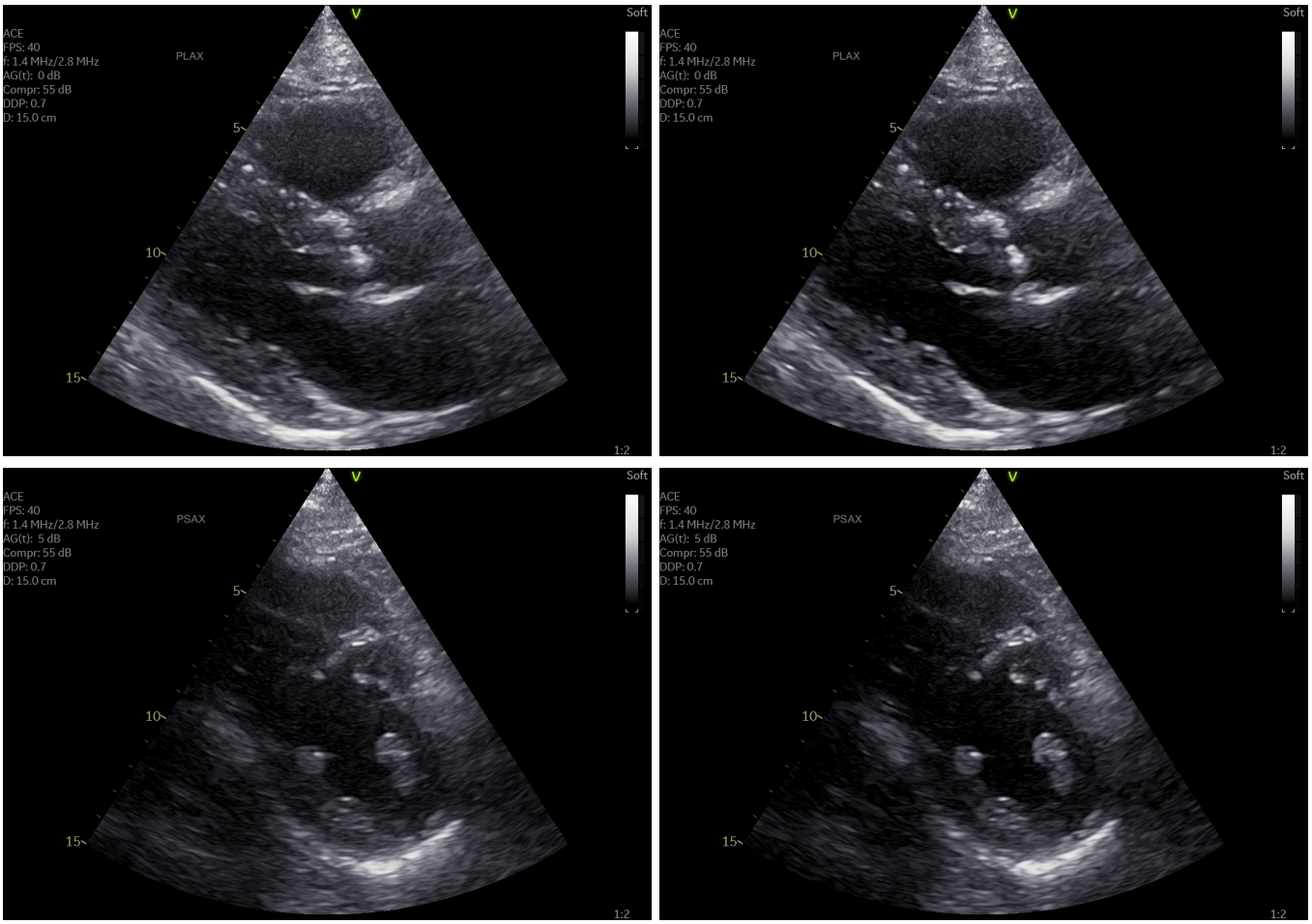

Fig. 4. Case example 1. Parasternal views from patient 10. Standard image to the left and aberration corrected image to the right. Top row PLAX view, and bottom row PSAX views.

Patient 10 is presented[1]

These images are here referred to as case example 1 (see Fig. 2). The standard image is displayed on the left and the aberration corrected image on the right. Aberration correction clearly improved all the images from this patient. In general, image contrast and sharpness is improved. The cardiac structures, including endocardial borders and valves, appear thinner and more clearly defined. This is particularly evident in the ALAX view (Fig. 5 bottom row) from this patient, where the mitral valve leaflets and endocardial borders become very clear after aberration correction. In the following, selected case examples are presented from all image views. The numbering of the case examples is provided in the legend of Fig. 2.

Selected frames for case examples 2, 3, and 7 are presented in Fig. 6. These three cases are the ones with the largest increase in the GIC parameter after aberration correction. Note also that these cases have an image quality around the median value of all images.

In case examples 2 and 3, the septal wall is almost not visible before aberration correction is applied. The images appear noisy prior to aberration correction, and there is a significant reduction of noise in the cavity as the signal intensity from the tissue is increased after aberration correction. Endocardial borders and valves are sharpened with a generally improved contrast with respect to the cavity.

Selected frames from case examples 4, 5, and 6 are presented in Fig. 7. As quantified by the GIC, case example 4 has above median image quality and obtains approximately median GIC improvement after processing with Adapt. Case examples 5 and 6 have the highest and close to lowest image quality, and both obtain some of the lowest increases in GIC after aberration correction. These numbers match well with the observed image quality and improvement after aberration correction in the displayed images. Still, the same trend is also visible here as for the other presented case examples with improved image contrast, endocardial borders and sharper structures (although very moderate improvements for case 5, but quite clear around the valve and the thin portion of the right ventricle visible in the upper right part of the image).

IV. Discussion

The aberration correction algorithm is shown to improve all images using the GIC parameter. The clinicians reported that

[1]Cineloops (at 50% replay speed) of all the presented case examples in this paper are provided online in the supplementary files. The Adapt image is always to the right. The cineloops are compressed and do not display as detailed images as the clinicians had access to in EchoPac.

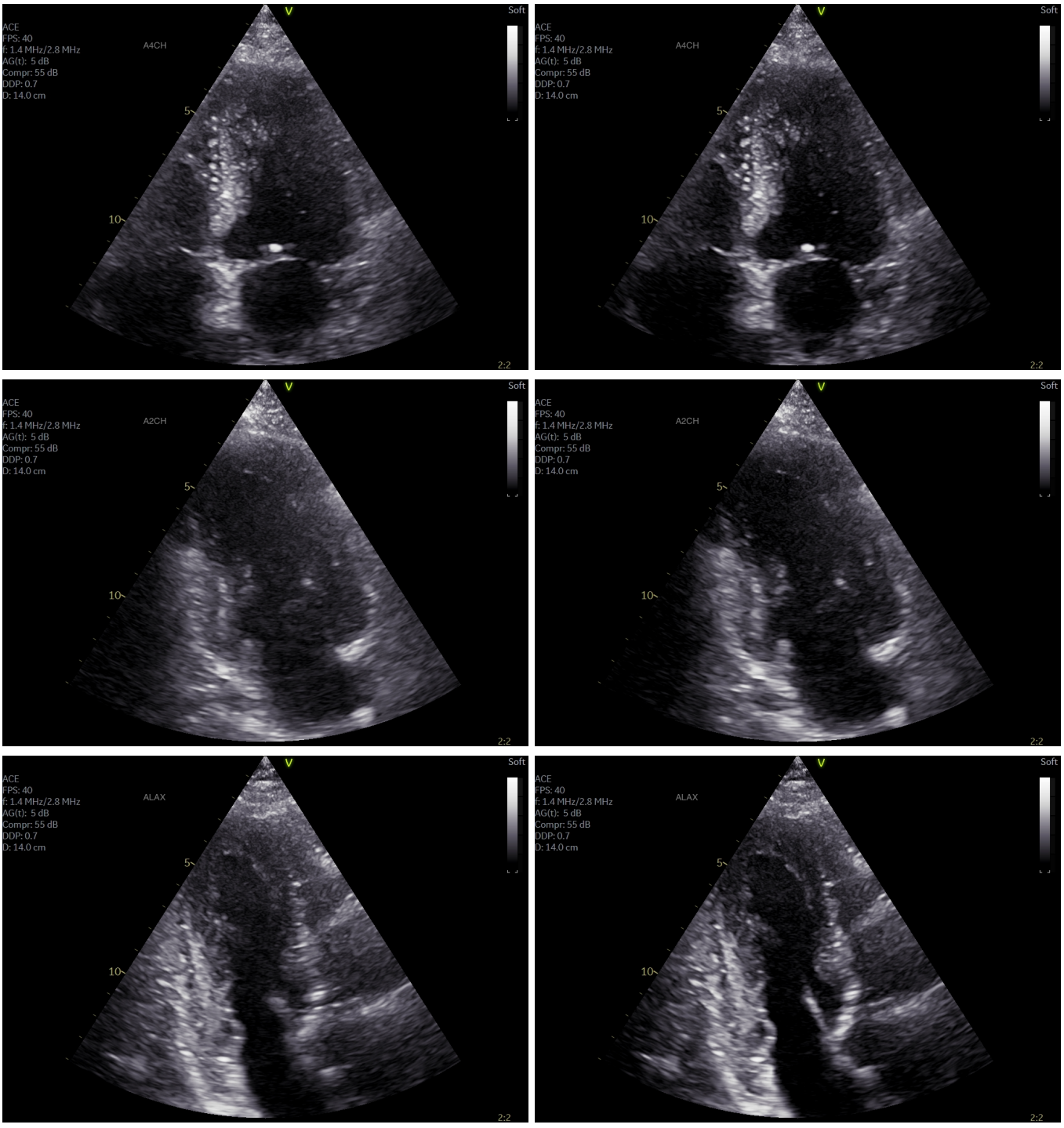

Fig. 5. Case example 1. Apical views from patient 10. Standard image to the left and aberration corrected image to the right. The rows display (from top to bottom) the A4C, A2C, and ALAX views respectively.

the aberration corrected images appeared sharper with better contrast and less noise. The corrected image was preferred in a blind comparison in 97 % of the cases. Many structures like valve leaflets, chordae, and the endocardium appear narrower and more clearly defined in the aberration corrected images. In many examinations the difference was clearly visible in the cineloops running at full speed. In a few of the cases, the improvements were apparent only at reduced replay speed or in still frames. In a few cases (in still frames), the clinicians reported that some parts of the image were improved while other parts were slightly degraded. The slight degradation was not deemed to be of clinical significance. Also, the algorithm was reported to be stable with no visible image artefacts in replay mode.

The image quality improvement varied by patient. This is expected. It is well known that image quality varies by patient,

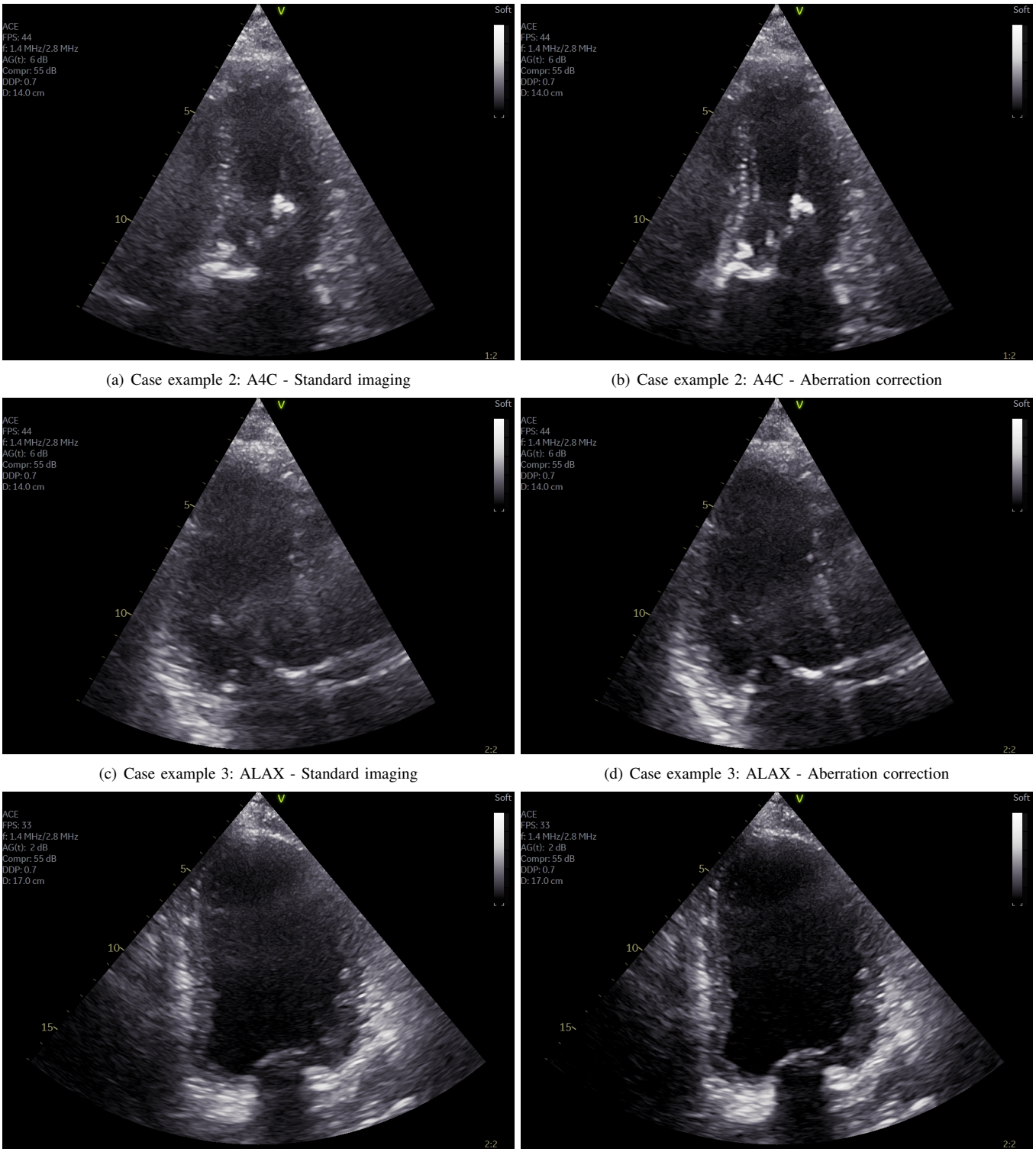

(a) Case example 2: A4C - Standard imaging

(b) Case example 2: A4C - Aberration correction

(c) Case example 3: ALAX - Standard imaging

(d) Case example 3: ALAX - Aberration correction

(e) Case example 7: A2C - Standard imaging

(f) Case example 7: A2C - Aberration correction

Fig. 6. Case example 2 (Patient 1), 3 (Patient 1) and 7 (Patient 20) (see Fig. 2).

so that the maximum image improvement is inherently patient-dependent. In addition, it is unlikely that adjusting beamforming time-delays can fully correct for all image degradation. As stated previously, the algorithm aims at compensating the effect of a variable speed of sound in the body wall. There are, however, several other acoustic effects degrading image quality in echocardiography such as reverberations, scattering and shadowing from ribs, lung and other structures. See, for example, Fatemi *et al.* [34]. A common denominator of these effects is clutter (or haze) overlying some or all of the ultrasound image. In the examples presented here, while clutter is also visible after aberration correction in many cases, it is

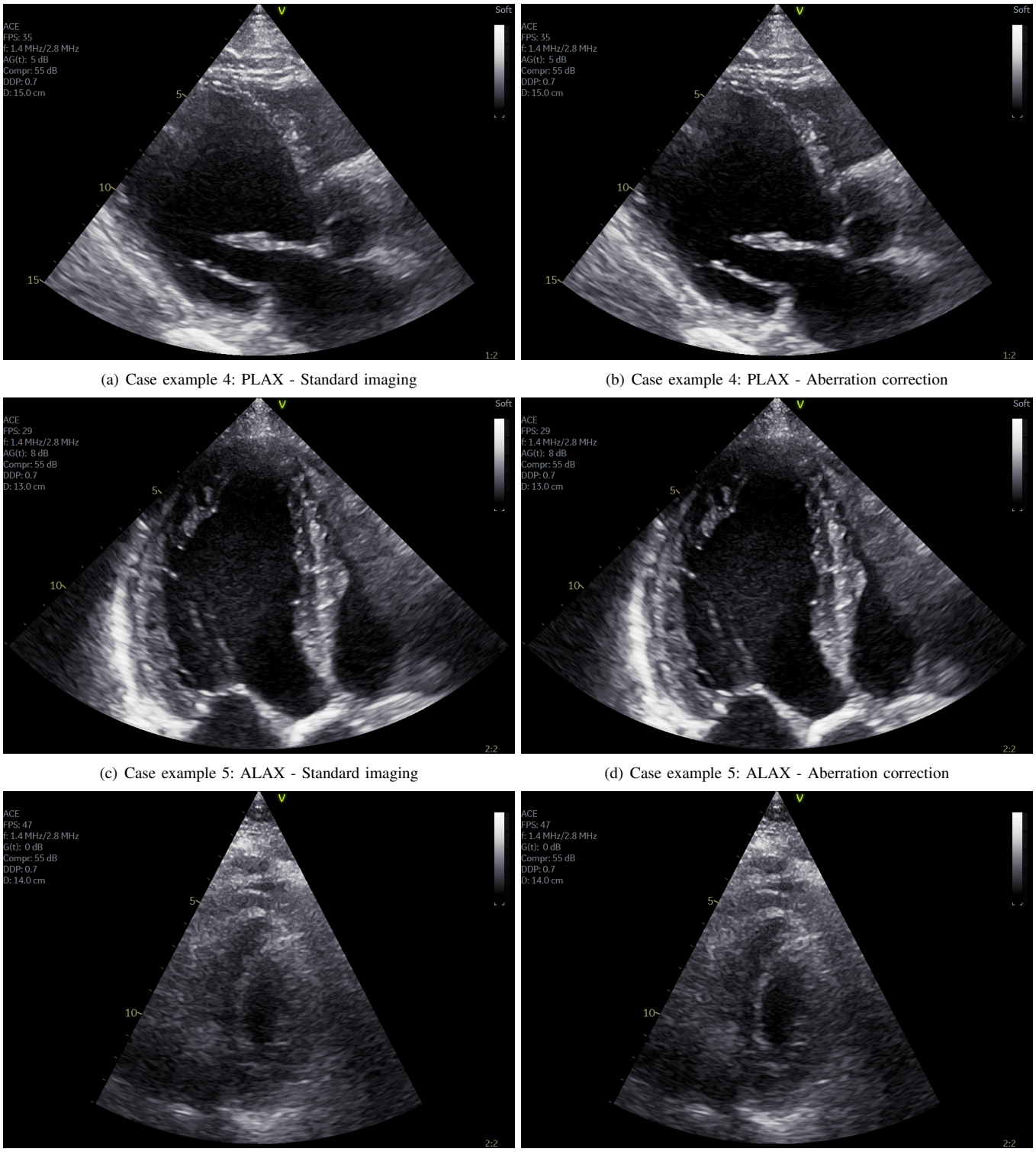

(a) Case example 4: PLAX - Standard imaging

(b) Case example 4: PLAX - Aberration correction

(c) Case example 5: ALAX - Standard imaging

(d) Case example 5: ALAX - Aberration correction

(e) Case example 6: PSAX - Standard imaging

(f) Case example 6: PSAX - Aberration correction

Fig. 7. Case example 4 (Patient 2), 5 (Patient 5) and 6 (Patient 15) (see Fig. 2).

also significantly reduced due to the increase in tissue intensity from the correction.

The GIC parameter correlates well with clinicians' assessment of image quality: the GIC increased with aberration correction in every instance, and the clinicians preferred the aberration-corrected cineloop in 97 % of the instances. This is particularly clear from case examples 5 and 6 (Fig. 7) which represent the cases with the highest and one of the lowest GIC parameter for all recorded cineloops.

Two of the clinicians (one experienced and one in training) preferred the aberration correction algorithm for all the analyzed cineloops. The two other clinicians preferred the

standard image in 2.4 % (11 cases in total), and one clinician found one case (0.2 %) to be of equal quality. It is not clear why the clinicians disagreed in these few instances. (They were not asked to review the results.) Since no criteria were agreed upon for defining image quality, it may simply reflect differences in personal preferences.

The focusing criterion defined by Mallart *et al.* [32] is almost identical to the Coherence Factor [33] used here, except for a range-averaging term. For a medium with delta-function spatial correlations, the focusing criterion is shown to be independent of frequency and probe aperture size in the focal region of the probe [32]. This assumption is not valid for coherent structures like the heart. Also, the Coherence Factor used here is calculated for the entire image range, meaning it is calculated also outside the probe transmit focal region. This renders the GIC dependent on image view. In principle, it is also dependent on the beamforming algorithm used by a specific system, meaning it is not straightforward to compare GIC values between systems or imaging modes. Still, for a given system, view dependent values of the GIC may be established and used for evaluating image quality.

Choosing to compensate for the gain increase generated by the aberration correction algorithm was carried out to make it more difficult for the clinicians to observe which image had been processed with the algorithm. Randomizing the images to the left and right without gain compensation created a pattern of brighter cardiac structures in the Adapt images which was easily detected by non-clinicians reviewing the images during testing of the evaluation procedure.

Several levels of pixel intensities were tested for the gain compensation method. Using 10 % or 30 % of the brightest pixels was also evaluated, but 20 % was deemed to be a good compromise. In some cases the chosen value could potentially reduce the gain a bit too much in the Adapt image, but in others too little. Overall, the method seemed to perform well as documented through case examples presented in this paper. The compensation varied between 0.5-2.2 dB, with a median value of 1.2 dB, a significant increase of tissue signal level after aberration correction.

V. Conclusion

This work shows that aberration correction is feasible and systematically improves images in pulse-echo imaging of the heart. A coherence metric [the Global Image-Coherence (3)], increased in all 7380 processed images after applying aberration correction. The results were validated by four clinicians selecting the image they preferred in a blinded and left-right-randomized side-by-side analysis of aberration-corrected versus non-aberration corrected images. The clinicians preferred the aberration corrected images in 97 % of the 116 analysed cineloops.

Aberration correction improved resolution and contrast in the images, yielding sharpened structures, thinner valves, cords, and improved endocardial border visualization. The improvement varied with patient and image view; the apical views obtained the largest improvements seen in the GIC but overall there was no statistically significant correlation of image improvement and image view.

Perhaps the most significant effect of aberration correction is improved cardiac tissue intensity, improving contrast in all images. This was quantified by a median gain increase in high intensity image pixels of 1.2 dB over all the 116 processed channel data cineloops. The gain increase was strongly correlated with increasing GIC in the aberration corrected images.

Aberration correction has here been shown to improve clinical echocardiography images. The improvement is systematic and may facilitate and improve clinical evaluation of echocardiograms and diagnosis of cardiac disease. Larger studies using Adapt are required to validate this hypothesis.

Acknowledgment

Many past employees of GE Research have worked to bring aberration correction to commercial ultrasound imaging. We would especially acknowledge the contributions of Carl Chalek, Bruno Haider, Matt O'Donnell and Doug Wildes.

References

[1] G. D. Ludwig, "The Velocity of Sound through Tissues and the Acoustic Impedance of Tissues," *The Journal of the Acoustical Society of America*, vol. 22, no. 6, pp. 862–866, Nov. 1950.

[2] M. E. Anderson and G. E. Trahey, "The direct estimation of sound speed using pulse–echo ultrasound," *The Journal of the Acoustical Society of America*, vol. 104, no. 5, pp. 3099–3106, Nov. 1998.

[3] Q. Chen and J. A. Zagzebski, "Simulation study of effects of speed of sound and attenuation on ultrasound lateral resolution," *Ultrasound in Medicine and Biology*, vol. 30, no. 10, pp. 1297–1306, Oct. 2004, publisher: Elsevier.

[4] D. E. Goldman and T. F. Hueter, "Tabular Data of the Velocity and Absorption of High-Frequency Sound in Mammalian Tissues," *The Journal of the Acoustical Society of America*, vol. 28, no. 1, pp. 35–37, Jan. 1956.

[5] S. A. Goss, R. L. Johnston, and F. Dunn, "Comprehensive compilation of empirical ultrasonic properties of mammalian tissues," *The Journal of the Acoustical Society of America*, vol. 64, no. 2, pp. 423–457, Aug. 1978.

[6] S.-E. Måsøy, T. F. Johansen, and B. Angelsen, "Correction of ultrasonic wave aberration with a time delay and amplitude filter," *The Journal of the Acoustical Society of America*, vol. 113, no. 4, pp. 2009–2020, Mar. 2003.

[7] T. D. Mast, L. M. Hinkelman, M. J. Orr, V. W. Sparrow, and R. C. Waag, "Simulation of ultrasonic pulse propagation through the abdominal wall," *The Journal of the Acoustical Society of America*, vol. 102, no. 2, pp. 1177–1190, Aug. 1997.

[8] L. M. Hinkelman, D. L. Liu, L. A. Metlay, and R. C. Waag, "Measurements of ultrasonic pulse arrival time and energy level variations produced by propagation through abdominal wall," *The Journal of the Acoustical Society of America*, vol. 95, no. 1, pp. 530–541, Jan. 1994.

[9] L. M. Hinkelman, T. D. Mast, L. A. Metlay, and R. C. Waag, "The effect of abdominal wall morphology on ultrasonic pulse distortion. Part I. Measurements," *The Journal of the Acoustical Society of America*, vol. 104, no. 6, pp. 3635–3649, Dec. 1998.

[10] T. D. Mast, L. M. Hinkelman, M. J. Orr, and R. C. Waag, "The effect of abdominal wall morphology on ultrasonic pulse distortion. Part II. Simulations," *J. Acoust. Soc. Am.*, vol. 104, no. 6, pp. 3651–3664, Dec. 1998.

[11] L. M. Hinkelman, D. Liu, R. C. Waag, Q. Zhu, and B. D. Steinberg, "Measurement and correction of ultrasonic pulse distortion produced by the human breast," *The Journal of the Acoustical Society of America*, vol. 97, no. 3, pp. 1958–1969, Mar. 1995.

[12] L. M. Hinkelman, T. L. Szabo, and R. C. Waag, "Measurements of ultrasonic pulse distortion produced by human chest wall," *The Journal of the Acoustical Society of America*, vol. 101, no. 4, pp. 2365–2373, Apr. 1997.

[13] R. S. Finkelhor, M. Moallem, and R. C. Bahler, "Characteristics and Impact of Obesity on the Outpatient Echocardiography Laboratory," *The American Journal of Cardiology*, vol. 97, no. 7, pp. 1082–1084, Apr. 2006.

[14] M. C. El Hajj and S. E. Litwin, "Echocardiography in the Era of Obesity," *Journal of the American Society of Echocardiography*, vol. 33, no. 7, pp. 779–787, Jul. 2020.
[15] M. Hirama, O. Ikeda, and T. Sato, "Adaptive ultrasonic array imaging system through an inhomogeneous layer," *The Journal of the Acoustical Society of America*, vol. 71, no. 1, pp. 100–109, Jan. 1982.
[16] S. Flax and M. O'Donnell, "Phase-aberration correction using signals from point reflectors and diffuse scatterers: basic principles," *IEEE Transactions on Ultrasonics, Ferroelectrics, and Frequency Control*, vol. 35, no. 6, pp. 758–767, Nov. 1988.
[17] M. O'Donnell and S. Flax, "Phase-aberration correction using signals from point reflectors and diffuse scatterers: measurements," *IEEE Transactions on Ultrasonics, Ferroelectrics, and Frequency Control*, vol. 35, no. 6, pp. 768–774, Nov. 1988.
[18] L. F. Nock, G. E. Trahey, and S. W. Smith, "Phase aberration correction in medical ultrasound using speckle brightness as an image quality factor," *J. Acoust. Soc. Am.*, vol. 85, no. 5, pp. 1819–1833, May 1989.
[19] D. Liu and R. C. Waag, "Correction of ultrasonic wavefront distortion using backpropagation and a reference waveform method for time-shift compensation," *The Journal of the Acoustical Society of America*, vol. 96, no. 2, pp. 649–660, Aug. 1994.
[20] C. Prada and M. Fink, "Selective focusing through inhomogeneous media: the DORT method," in *1995 IEEE Ultrasonics Symposium. Proceedings. An International Symposium*, vol. 2, Nov. 1995, pp. 1449–1453 vol.2, iSSN: 1051-0117.
[21] A. P. Berkhoff and J. Thijssen, "Correction of concentrated and distributed aberrations in medical ultrasound imaging," *1996 IEEE Ultrasonics Symp. Proc.*, vol. 2, pp. 1405–1410, 1996.
[22] S. Krishnan, K. W. Rigby, and M. O'Donnell, "Efficient Parallel Adaptive Aberration Correction," *IEEE Trans. Ultrason. Ferroelectr. Freq. Control*, vol. 45, no. 3, pp. 691–703, May 1998.
[23] S.-E. Måsøy, B. Angelsen, and T. Varslot, "Estimation of ultrasound wave aberration with signals from random scatterers," *The Journal of the Acoustical Society of America*, vol. 115, no. 6, pp. 2998–3009, Jun. 2004.
[24] T. Varslot, H. Krogstad, E. Mo, and B. A. Angelsen, "Eigenfunction analysis of stochastic backscatter for characterization of acoustic aberration in medical ultrasound imaging," *The Journal of the Acoustical Society of America*, vol. 115, no. 6, pp. 3068–3076, Jun. 2004.
[25] R. Waag and J. Astheimer, "Statistical estimation of ultrasonic propagation path parameters for aberration correction," *IEEE Transactions on Ultrasonics, Ferroelectrics, and Frequency Control*, vol. 52, no. 5, pp. 851–869, May 2005.
[26] E. Herbert, M. Pernot, G. Montaldo, M. Fink, and M. Tanter, "Energy-based adaptive focusing of waves: application to noninvasive aberration correction of ultrasonic wavefields," *IEEE Transactions on Ultrasonics, Ferroelectrics, and Frequency Control*, vol. 56, no. 11, pp. 2388–2399, Nov. 2009.
[27] B.-F. Osmanski, G. Montaldo, M. Tanter, and M. Fink, "Aberration correction by time reversal of moving speckle noise," *IEEE Transactions on Ultrasonics, Ferroelectrics, and Frequency Control*, vol. 59, no. 7, pp. 1575–1583, Jul. 2012.
[28] W. Lambert, L. A. Cobus, M. Fink, and A. Aubry, "Ultrasound Matrix Imaging. II. The distortion matrix for aberration correction over multiple isoplanatic patches," *arXiv:2103.02036 [physics]*, Mar. 2021.
[29] H. Bendjador, T. Deffieux, and M. Tanter, "SVD beamforming for ultrafast aberration correction and real-time speed-of-sound quantification," in *2020 IEEE International Ultrasonics Symposium (IUS)*, Sep. 2020, pp. 1–4, iSSN: 1948-5727.
[30] K. W. Rigby, C. L. Chalek, B. H. Haider, R. S. Lewandowski, M. O'Donnell, L. S. Smith, and D. G. Wildes, "Improved In Vivo Abdominal Image Quality Using Real-time Estimation and Correction of Wavefront Arrival Time Errors," *IEEE Ultrasonics Symposium*, vol. 2, pp. 1645–1653, Oct. 2000.
[31] A. Østvik, E. Smistad, S. A. Aase, B. O. Haugen, and L. Løvstakken, "Real-Time Standard View Classification in Transthoracic Echocardiography Using Convolutional Neural Networks," *Ultrasound in Medicine & Biology*, vol. 45, no. 2, pp. 374–384, Feb. 2019.
[32] R. Mallart and M. Fink, "Adaptive focusing in scattering media through sound-speed inhomogeneities: The van Cittert Zernike approach and focusing criterion," *The Journal of the Acoustical Society of America*, vol. 96, no. 6, pp. 3721–3732, Dec. 1994.
[33] K. Hollman, K. Rigby, and M. O'Donnell, "Coherence factor of speckle from a multi-row probe," vol. 2, Oct. 1999, pp. 1257–1260 vol.2.
[34] A. Fatemi, E. A. R. Berg, and A. Rodriguez-Molares, "Studying the Origin of Reverberation Clutter in Echocardiography: In Vitro Experiments and In Vivo Demonstrations," *Ultrasound in Medicine & Biology*, vol. 45, no. 7, pp. 1799–1813, Jul. 2019.